

Flexible and Printed Electronics



PAPER

Intensive pulsed light sintered flexible conductive hybrid ink in 3D printed polymers

RECEIVED
26 September 2019

REVISED
17 November 2019

ACCEPTED FOR PUBLICATION
7 January 2020

PUBLISHED
27 January 2020

A Sandwell , Z Kockerbeck, C I Park, M Hassani, R Hugo and S S Park¹

Department of Mechanical and Manufacturing Engineering, University of Calgary, Calgary, Canada

¹ Author to whom any correspondence should be addressed.

E-mail: sipark@ucalgary.ca

Keywords: IPL sintering, copper ink, sensor, flexible

Abstract

The deposition of electrically conductive electrodes and circuits onto polymeric materials is essential for embedded sensors and circuits. A hybrid copper ink consisting of graphene nanoplatelets and silver-coated copper nanopowders are developed for oxidation resistance and increased flexibility. To prevent thermal damages to polymeric substrates, we used an intensive pulsed light (IPL) to sinter the hybrid ink. The IPL process is analyzed to determine thermal characteristics during the sintering of hybrid inks and to correlate IPL irradiance power to sintering depth and resulting resistivity within the hybrid ink film. The benefit of adding graphene nanoplatelets (GnP) into the hybrid ink is also demonstrated in improved flexibility and durability in the bending tests. A process called selective IPL sintering is also utilized to micropattern the hybrid ink films into useful conductive patterns. The proposed method is demonstrated in an additive process where we embedded a strain sensor within a functional 3D printed polymer structure.

1. Introduction

Printed electronics have gained considerable attention lately due to the rising demand for flexible electronic devices such as flexible displays, wearable technology, organic transistors, RFID tags, and flexible sensors [1]. Traditionally, printed circuits boards are fabricated using the photolithographic process involving etching [2]; however, this method is costly, relatively slow, requires special equipment and uses chemicals that are potentially harmful to the environment.

Recently, the deposition and sintering of metallic nanoparticles directly onto flexible polymers have been a focus of study for creating electrodes and interconnects. These conductive films are created either by inkjet printing or direct deposition onto typically polymeric substrates. In conventional sintering, metallic nanoparticles require high temperature to induce electrical conductivity. This limits the use of low-temperature polymeric substrates due to possible damage to the substrates in the sintering process.

The deposited metals often include gold and silver nanoparticles or nanowires; however, these metals are not cost-effective for most applications [3]. Copper nanoparticles, on the other hand, are significantly

cheaper while having similar electrical resistivity properties but are prone to oxidation in air environments.

To overcome high costs, fast oxidation, and low-temperature polymeric substrate limitations, we have developed a hybrid copper-silver nanoparticle ink that utilizes a combination of silver coating via galvanic reactions and intensive pulsed light (IPL) based sintering. The IPL based sintering exhibits extremely short exposure time (a few milliseconds) to sinter metallic particles, minimizing thermal damage to the substrates which is particularly useful for the use of low-temperature polymeric substrates such as PET, PE, and others [4].

The objectives of this study are to investigate the IPL sintering of hybrid copper inks and to integrate the inks with 3D printed polymeric materials for practical applications. The effects of the hybrid ink composition and the variation of the IPL input energy level on the resulting depth and the electrical resistivity are experimentally investigated. The benefits of the graphene nanoplatelet (GnP), on the overall flexibility and durability of the sintered ink trace, is also explored. The temperature in the IPL sintering process is estimated using a simplified finite element (FE) model and compared with the experimental measurement.

Table 1. Hybrid copper ink compositions.

	Cu (g)	AgNO ₃ (g)	GNP (g)	PVP (g)	HCOOH (ml)	DEG (ml)
Ink A (CS)	2	0.15	0	0.12	8	2
Ink B (CSG)	2	0.15	0.2	0.12	8	2

To integrate the hybrid ink with 3D printing, the ink is directly deposited on to a 3D printed part, selectively sintered, and encased by another 3D printed part. The selective IPL sintering is utilized to generate a strain gauge pattern onto the deposited film by blocking the IPL energy using a metallic mask. The concept of hybrid copper conductive inks with IPL sintering process was verified to be an efficient and effective method to produce flexible electronic sensors embedded within 3D printed structures.

2. Experimental

2.1. Materials and ink film preparation

The hybrid conductive copper inks are produced by combining metallic nanoparticles (copper, tin, and zinc), silver nitrate for silver coating and GnPs for enhanced conductivity in flex. Formic acid treatment is utilized to prevent copper oxide formation. A polymer carrier is also added to provide increased flexibility and durability to the ink.

For the preparation of the hybrid copper inks, the copper nanoparticles (Cu NPs) of 100 nm average diameter (Tekna) are mixed with silver nitrate (AgNO₃), poly-(N-vinylpyrrolidone) (PVP, MW: 40 000 g mol⁻¹), diethylene glycol (DEG), and formic acid (HCOOH). The variant of ink was also made by first adding GnPs (specific surface area: 500 m² g⁻¹). Table 1 describes the detailed compositions of the inks used in this study.

Metallic nanoparticles are treated and mixed with an aqueous solution of formic acid, using both vortex mixing and sonication. The formic acid serves to generate copper formate and further remove the oxide layer from the copper nanoparticles. The entire mixture is then added to a solution of DEG and poly-(N-vinylpyrrolidone) (PVP) along with silver nitrate. The silver nitrate reacts with the copper nanoparticles to form a solid silver coating via a galvanic replacement reaction. The resulting solution is stirred well before application for dispersion [4].

The created inks can be applied to a variety of substrates. In this study, the doctor blade method is applied to deposit the inks onto a soda-lime glass and PET (IBM 24L5255) for experimental investigations, and onto Acrylonitrile Butadiene Styrene (ABS) for the embed sensor application. The film is dried at 120 °C on a hotplate for 10 min to remove any residual solvents. The hybrid inks are then sintered using IPL treatment (see figure 1) to form a conductive network between deposited particles.

An intensive light pulse from the Xenon flash tube (Cerium Type A, Xenon S-2300) sinters the hybrid ink, as shown in figure 1(a). The spectrum band of IPL ranges from 350 to 1050 nm, as shown in figure 1(b). The wide range of spectrum allows high energy absorption by the hybrid ink specimen.

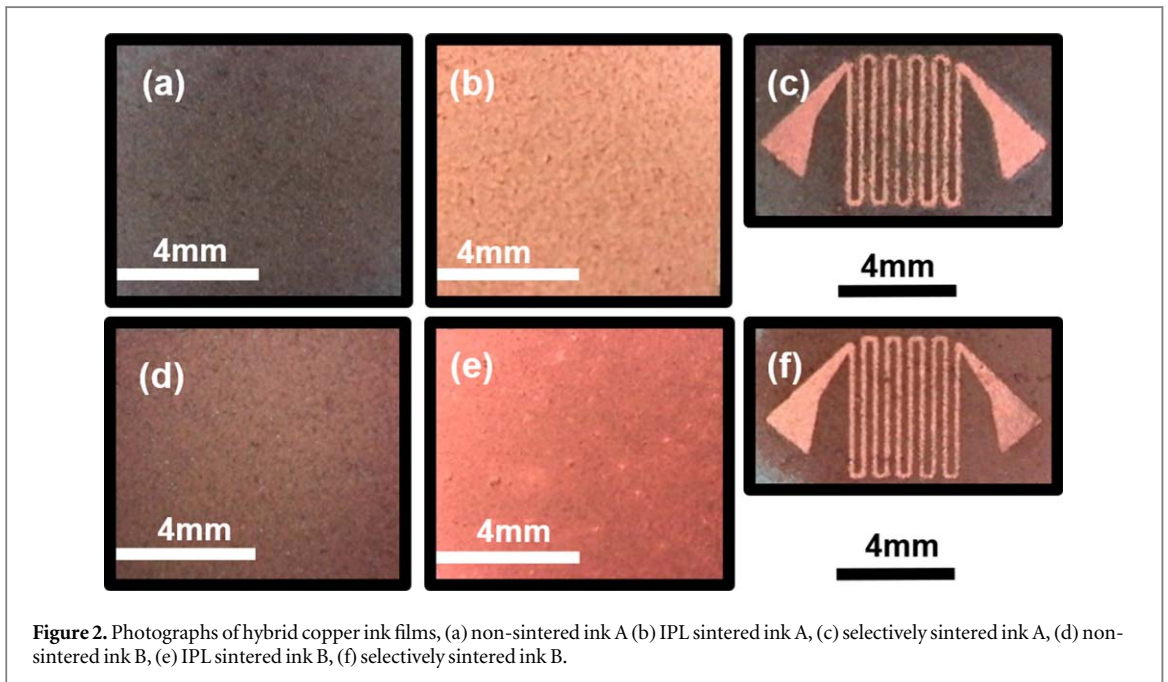
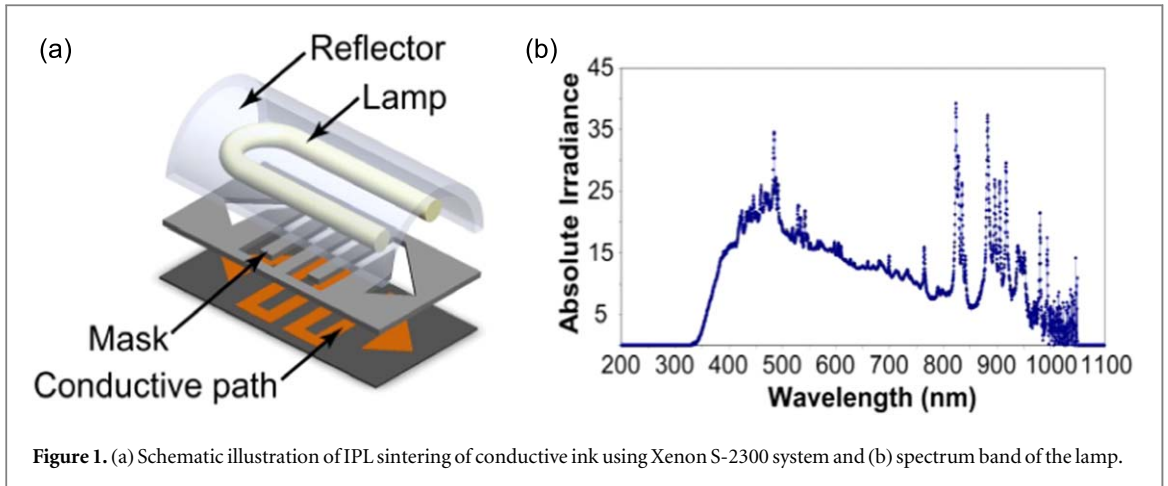
With the precise control of pulse, two different square-shaped pulses of 1 and 2.5 ms duration were applied to the samples. The input voltages for 1 ms pulse were varying from 2400 to 3000 V with the increment of 150 V, corresponding to the sintering energy density of 0.86–1.46 J cm⁻². For the sintering process with 2.5 ms pulse, the input voltage ranged from 1800 to 3000 V with the increment of 150 V, corresponding to the energy density of 1.07–3.66 J cm⁻². The pulse duration and increment energy density settings were experimentally determined to analyze ink A and ink B with different levels of sintering.

The direct effect of IPL sintering on the hybrid inks is shown in figure 2. Before the sintering, the deposited hybrid inks are nonconductive and dark brown (see figures 2(a), (d)). Exposing the deposited ink to the xenon flash then induces sintering, resulting in the changes of conductivity in the exposed area. The change of color from dark brown to bright copper indicates that the exposed area has been sintered (see figures 2(b), (e)). In order to create a strain gauge, a chemically machined nickel mask is placed over the top of the hybrid ink films (see figures 2(c), (f)). The exposed hybrid inks then become micropatterned with a conductive circuit after the IPL.

2.2. Experimental procedures

Due to the nature of the IPL process, the hybrid copper inks may only partially sinter, forming a conductive layer at the surface of the film where the energy is directly applied. To accurately measure the resistivity of the sintered ink, it is required to find out the sintered depth of the ink in each experiment.

Measurement of the sintered depth of the ink is performed by observing the cross-section of the deposited hybrid ink films. First, the sintered hybrid copper ink films are encased in epoxy and cut perpendicular to the sample surface using a diamond saw, creating an exposed cross-section. After polishing down to 5 μm using a diamond lapping paste to expose the ink cross-section, the samples are imaged using an optical 3D profilometer (Zeta-20) to determine the depth of sintering. The sheet resistance of Ink A and Ink B conductive films were measured using a 4-probe multi-meter (34460 A, Keysight). The resistivity was calculated from the sheet resistance and the thickness



of the sintered film. The surface was also observed using a 3D optical profilometer (Zeta-20) and a scanning electron microscope (SEM).

Since the inks are designed for strain sensing applications, the deposited films should be resistant to mechanical damages due to repeated cycles of stress and strain. To characterize the durability of each sample, ink A and ink B samples undergo cyclic bending tests using a tensile tester (Mark-10 ESM303) and a 2-probe multi-meter to compare the changes in resistance values after multiple cycles. To accurately compare the performance of the two ink films, 15 mm by 10 mm films are deposited onto 45 mm × 10 mm textured PET substrates (IBM 24L5255) where the adhesion is maximized to minimize microcracking during bending.

Both films undergo 1000 bending cycles while the resistance is measured every 100 cycles. A bending radius of 3 mm is calculated for the films by utilizing the equation below:

$$r = \frac{L}{2\pi \sqrt{\frac{dL}{L} - \frac{\pi h_s^2}{12L^2}}}, \quad (1)$$

where L , the distance between the grips on the Mark-10 tensile tester, is 15 mm, dL , the movement of the upper grips, is 9.5 mm, and h_s , the thickness of the PET substrate, is 0.1 mm. The bending test setup is shown in figure 3. As it is shown in figure 3, three samples are mounted at each bending test, collecting data from total of six different samples for each type of ink to find the average values.

In order to study the mechanisms of flashlight sintering of Cu nano- and micro-ink films in-depth, the temperature changes during the flashlight sintering process were also monitored. *In situ* temperature monitoring with a specialized thermo-couple-based circuit and a high-rate data acquisition system was used since the sintering process lasts only for a few milliseconds. Thermocouples with a 50 μm junction (Lab supplies, UK) were used to maximize response, and

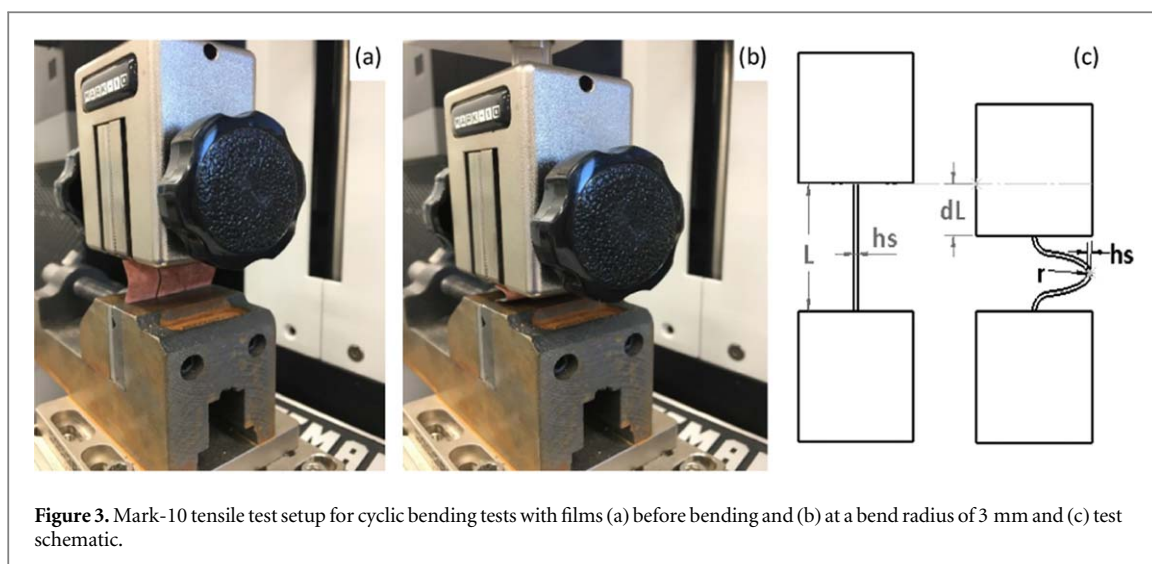


Figure 3. Mark-10 tensile test setup for cyclic bending tests with films (a) before bending and (b) at a bend radius of 3 mm and (c) test schematic.

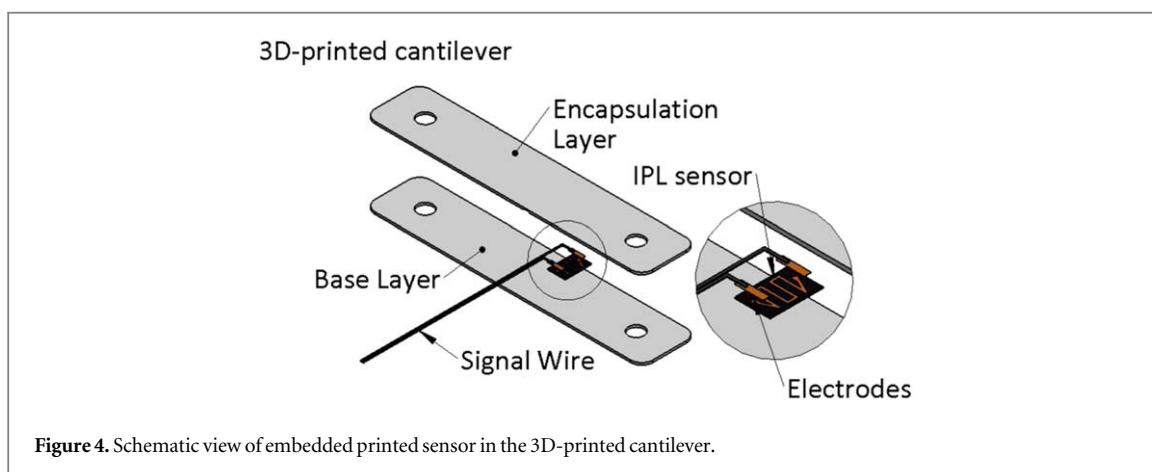


Figure 4. Schematic view of embedded printed sensor in the 3D-printed cantilever.

the measurement was amplified using a thermocouple amplifier signal conditioner module (HGSI). The resulting analog signal was passed to a DAQ (National Instruments) where the signal was captured and recorded to a computer.

The integration of hybrid copper inks with 3D printing is demonstrated by applying micro-patterned strain gauge design into a 3D printed ABS cantilever beam. A 3D printer (Flashforge 3D) fabricated a 130 mm by 25 mm by 3 mm cantilever beam, paused at half-way for direct ink deposition. The ink is deposited on top of the lower half of the cantilever beam, then selectively sintered using the IPL process. The 3D printing is re-started to print the remaining top layer, encasing the copper ink pattern within the cantilever. The embed circuit within the beam leads to exposed conductive ends for wiring (see figures 4 and 5).

The produced micro-patterned strain sensors are connected based on a Wheatstone full-bridge configuration and compared against an actuation reference. The comparison was performed using a vibration test (see figure 5) where a shaker (B&K 4808) is connected to a function generator (BK Precision 2053), power amplifier (B&K 2712) and a data acquisition system

(DAQ, NI 9237) measuring the strain gauge signals at 50 Hz vibration frequency.

3. Results and discussion

The effect of varying IPL energy density on the two different inks are described through the measurements of sintered depths, resistivity, and surface imaging. The effect of adding GnP on the cyclic bending performance of the films is also characterization. The resulting effect of IPL power variation is explained through with a simplified FE model of temperature changes with ink film. The optimal IPL sintering parameter is used to integrate the copper hybrid ink as a strain sensor within the 3D printed cantilever and experimentally verified against an actuation reference.

3.1. Electrical and optical analysis

To optimize the IPL process, the effect of how the xenon flash light transforms the ink film is characterized. The energy levels of IPL system were varied to examine the change in sintering depth and corresponding electrical resistivity. The deeper penetration of sintered depth is possible through the high-energy

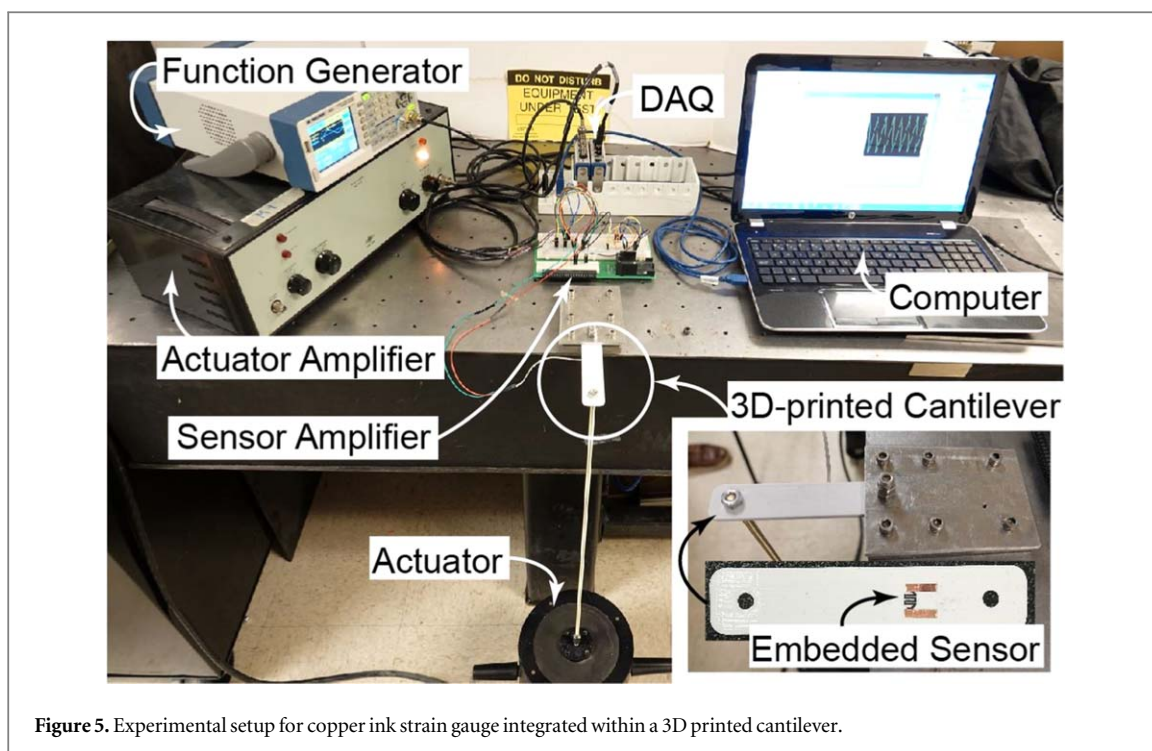


Figure 5. Experimental setup for copper ink strain gauge integrated within a 3D printed cantilever.

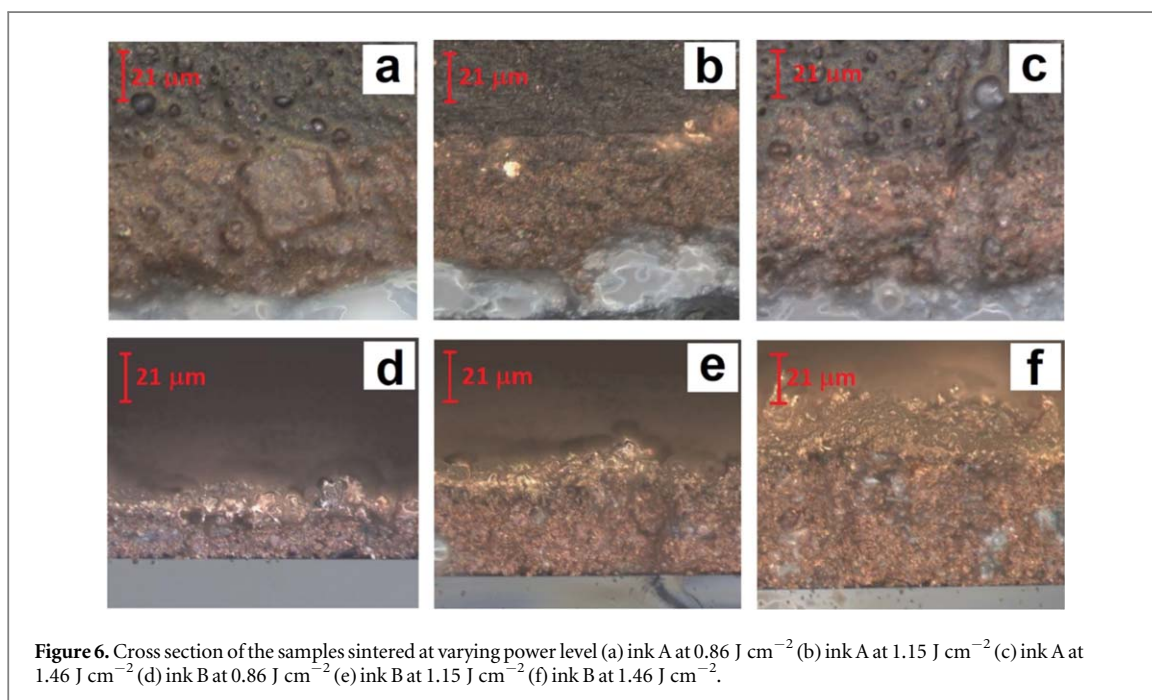


Figure 6. Cross section of the samples sintered at varying power level (a) ink A at 0.86 J cm^{-2} (b) ink A at 1.15 J cm^{-2} (c) ink A at 1.46 J cm^{-2} (d) ink B at 0.86 J cm^{-2} (e) ink B at 1.15 J cm^{-2} (f) ink B at 1.46 J cm^{-2} .

irradiation on the ink where extra energy transfers into the conductive ink film.

The cross section of hybrid ink samples show distinguishable layers of epoxy potting, sintered ink (marked with dotted lines), non-sintered ink and the glass substrate. The layers are not perfectly flat and the thickness varies slightly; ten different measurement points were taken for each condition to obtain average sintered depths.

At the same energy density level of 0.86 J cm^{-2} , Ink A exhibited the average sintered layer depth of $50 \mu\text{m}$ while Ink B had an average sintered layer depth

of $30 \mu\text{m}$. Figures 6 and 7 shows the relationship between the increasing sintering energy density and the increasing depth of sintered conductive inks, while electrical resistivity decreases as the sample is sintered.

The rapid drop in electrical resistivity is the sign of the sintering threshold energy. Ink A has its sintering threshold at the energy density of approximately 1.03 J cm^{-2} and Ink B is as low as 0.62 J cm^{-2} (occurred at pulse duration of $500 \mu\text{s}$), approximately a 40% reduction in required energy. The lowest resistivity achieved by Ink A is $0.17 \mu\Omega \text{ m}$ while the lowest resistivity achieved by Ink B is $1.15 \mu\Omega \text{ m}$.

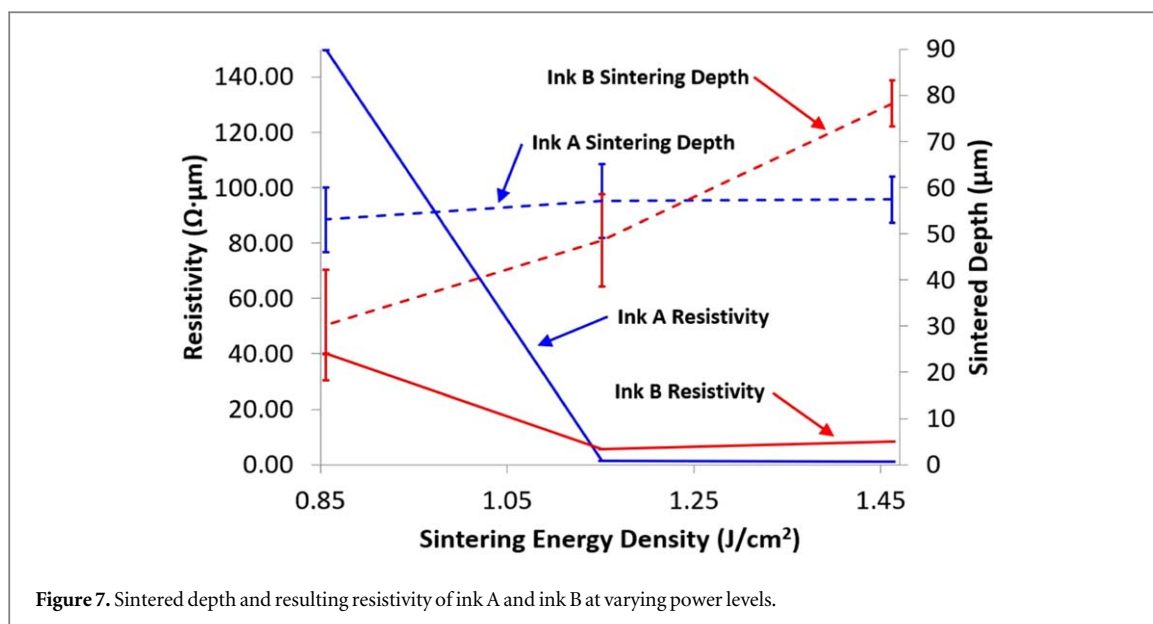


Figure 7. Sintered depth and resulting resistivity of ink A and ink B at varying power levels.

The surface morphologies of samples are investigated using SEM imaging (figure 8) to provide more information of the surface sintering effects on Ink A and B.

By observing the SEM images of the non-sintered samples, it was shown that copper formate ($\text{Cu}(\text{HCOO})_2$) crystal structures are embedded in copper nanoparticles in both ink samples. After the flash sintering using the minimum required energy, the copper formate crystals begin to decompose (figures 8(b), (e)). They are decomposed when the optimal level of power was irradiated (figures 8(c), (f)). The SEM images also show that the copper nanoparticles begin to neck and create conductive networks as the level of irradiance increases for both inks.

The major difference between the two inks is the presence of GnP in ink B. In ink B, the GnP acts as a surface for copper nanoparticles and copper formate to attach to in a 3D structure. As figures 8(e), (f) show, when the copper nanoparticles begin to neck as they are sintered, they also bond to the surface of the GnP. This creates a more durable and flexible microstructure compared to the long fragile sintered copper 'necks' in ink A, especially shown in figure 8(c). The contrast in two microstructures leads to the expectation that the ink B with GnP will have increased durability and flexibility compared to ink A.

Copper oxide (CuO) peaks are often observed at $2\theta = 32.6^\circ$, 34.0° and 36.4° corresponding to (110), (002) and (111) [5, 6]. These peaks are observed in the XRD pattern before IPL, as shown in figure 9. These peaks no longer appear in XRD after IPL validating that IPL can help to reduce non-conductive CuO components. Furthermore, IPL also helps to revert copper formate to copper metal. This is seen by the reduction in peak intensity for $2\theta = 18.5^\circ$ corresponding to the (111) phase of copper formate [7]. The silver peaks are observed at $2\theta = 38.2^\circ$, 47.4° , 64.6° and 77.4°

corresponding to (111), (200), (220) and (311), respectively [8]. The copper nanoparticle peaks can be observed at $2\theta = 43.5^\circ$, 50.6° and 74.2° corresponding to the (111), (200) and (220) peaks of copper nanoparticles, respectively [9].

3.2. Mechanical durability analysis

For integration with 3D printed parts, the hybrid copper inks need to be flexible to a certain degree in order to avoid damage during strain. The hybrid copper-silver ink (Ink A) is relatively fragile and easily fail under bending stresses. The addition of GnP into the hybrid ink (Ink B) allows increased flexibility during strain while still being sensitivities enough to measure resistance changes. In order to characterize the benefit of adding GnP into the hybrid inks, we performed cyclic bending tests using a tensile tester where the films underwent a thousand bending cycles. Figure 10 shows the plots of average normalized resistance (r/r_0) values over increasing number of bending cycles for each ink, sintered with the energy density of 1.15 J cm^{-2} .

After the first 100 cycles, the average resistance for the ink A begins to deviate from the initial resistance of 1.45 ohms. The resistance continues to increase as the film continues to bend, up to approximately 550% of the initial resistance after 1000 cycles. The increased resistance can be explained by the increasing amounts of microcracks on the surface. On the other hand, the ink B with added GnP shows a minimal increase in resistance even after 1000 cycles. It increased to the resistance value of 128% of original resistance, which is significantly less than the resistance increase shown in ink A. The bending tests demonstrate the effects of adding GnP to increase the overall durability of the hybrid inks. This result can be correlated to the SEM images in figure 8, where the copper nanoparticles appear to bond to the GnP.

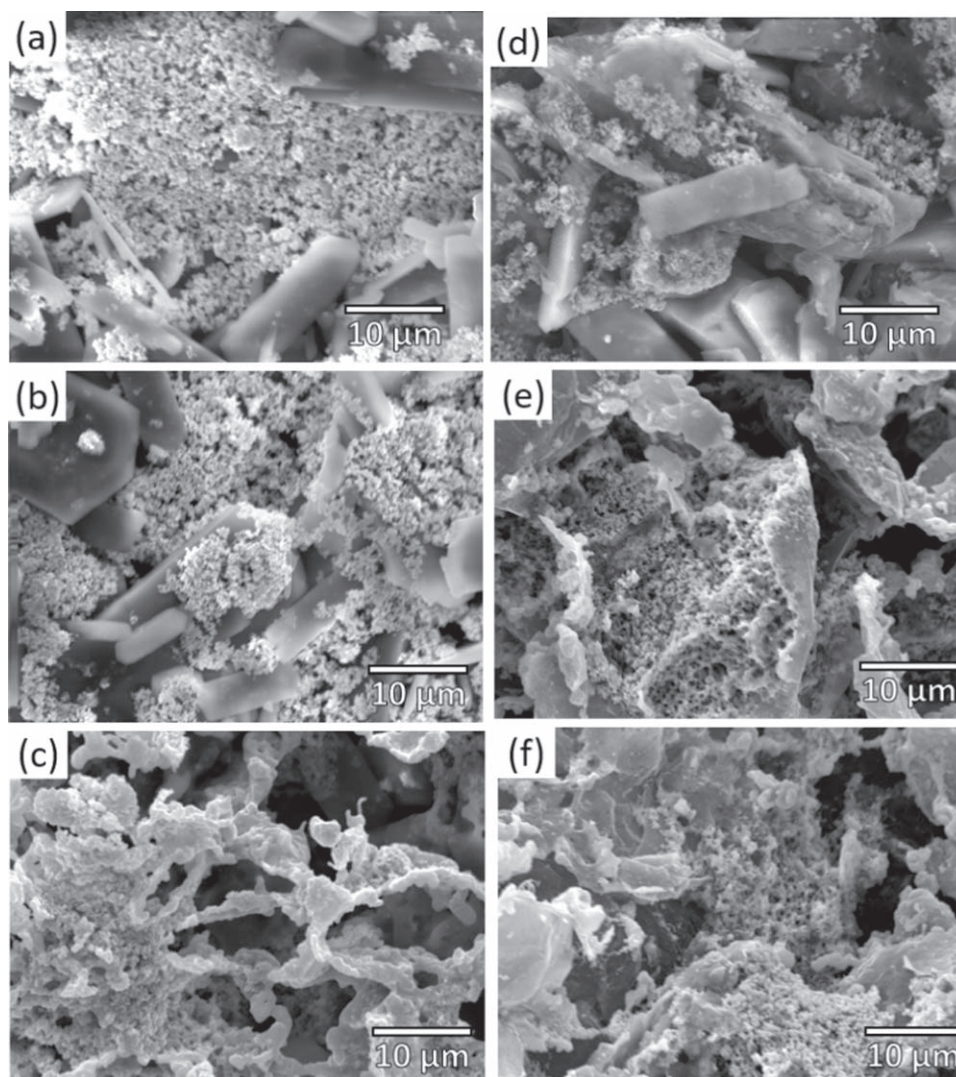


Figure 8. SEM images of hybrid inks: (a) non-sintered Ink A, (b) Ink A at 1.15 J cm^{-2} , (c) Ink A at 1.46 J cm^{-2} , (d) non-sintered Ink B, (e) Ink B at 1.55 J cm^{-2} , and (f) Ink B at 2.84 J cm^{-2} .

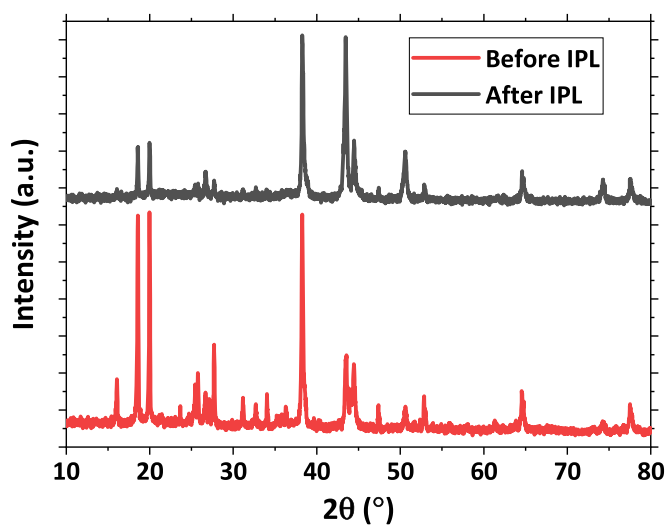
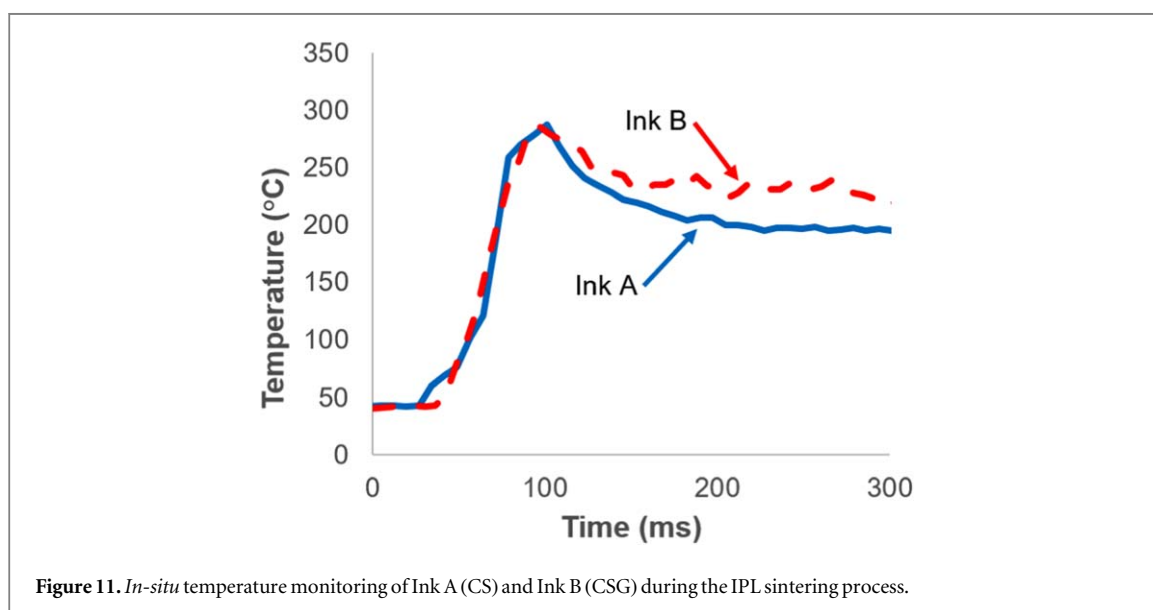
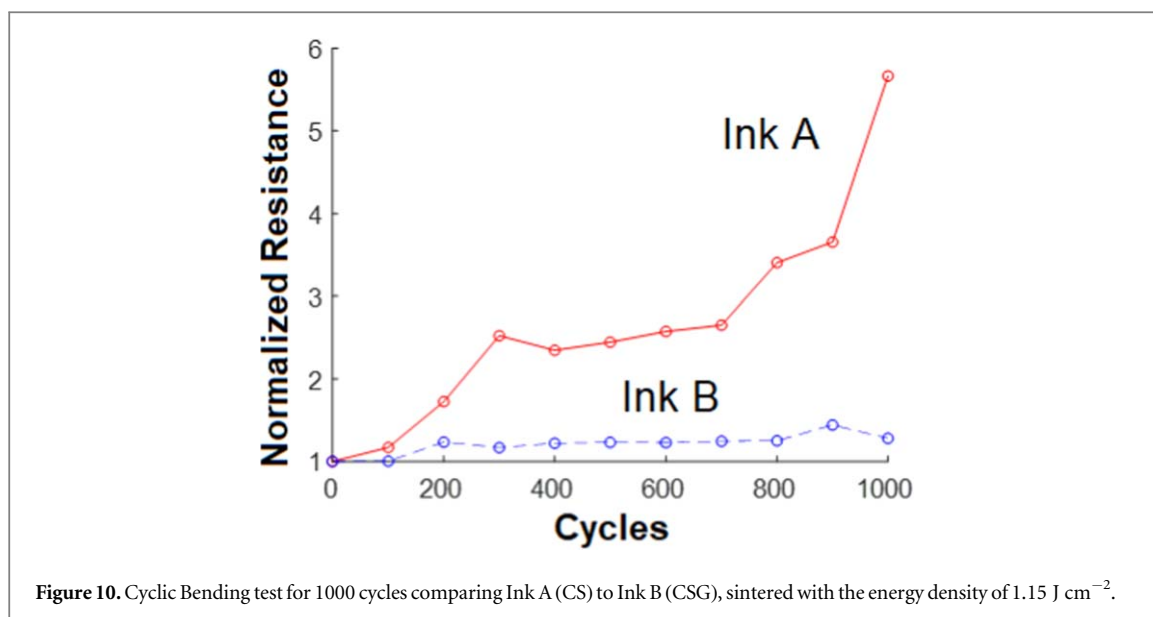


Figure 9. XRD pattern of ink B before and after IPL.



3.3. Thermal analysis

While the ink B with GnPs showed superior flexibility and durability compared to the ink A, it must be noted that the minimum required sintering energy also increased. Although it has the higher durability against multiple bending cycles, it is generally not suitable for applications with thermally weak polymer substrates if the maximum temperature is too high during the sintering process. Therefore it is important to identify not only the sintering energy, but also the maximum temperature at the irradiated samples.

The temperature of the IPL sintering process, however, is difficult to determine experimentally. First, the small window of time of the light pulse makes it difficult to measure the temperature changes. Also the direct irradiation of the light affects the temperature measuring devices, especially the infrared laser thermocouples.

However, few researchers have found the sintering temperature of copper nanoparticles experimentally despite the challenges. Park and others [10] used a K-type thermocouple with 1 ms response time and embedded the thermocouple in the substrate, measuring the temperature from the bottom of the sintered conductive layer. They reported that copper nanoparticle sintering starts somewhere between 407 and 547 K by indirectly calculating the surface temperature with an analytical transient heat transfer model [10]. Mittal and Jung [11] also found that copper nanoparticles of 20 nm diameter rigorously sinter at the temperature ranging from 490 to 507 K using high-resolution TEM and calorimeter, although it was not the IPL sintering process.

In this study, the *in situ* temperature monitoring of the IPL sintering was performed utilizing a thermocouple-based circuit and a high-rate data acquisition system. Figure 11 illustrates the temperature of ink A

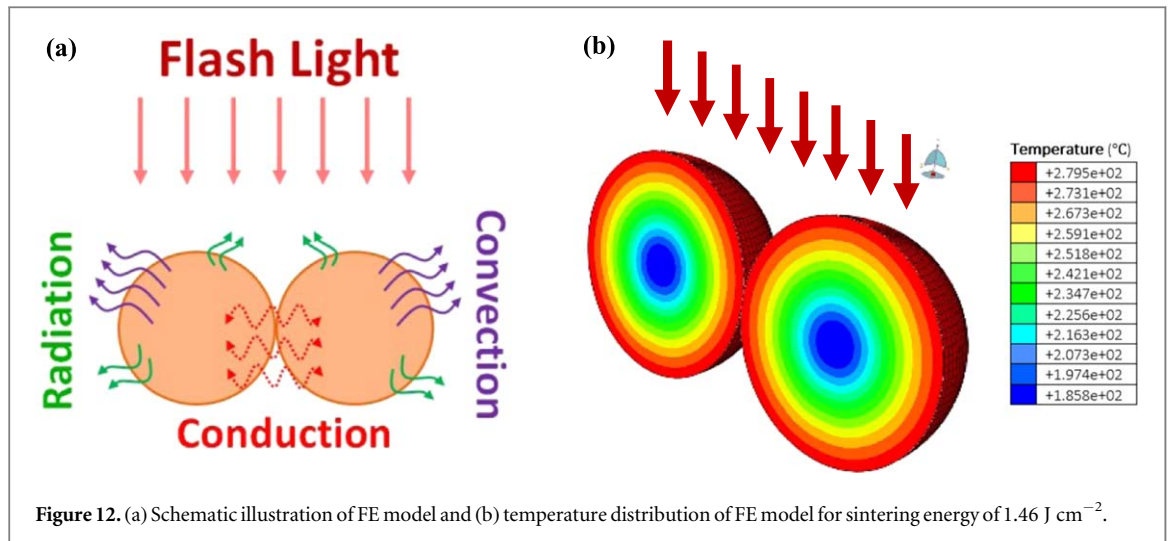


Figure 12. (a) Schematic illustration of FE model and (b) temperature distribution of FE model for sintering energy of 1.46 J cm^{-2} .

and B films increased instantly with flash light irradiation. Interestingly, the maximum temperature of sintering process was approximately 573 K for both ink samples. The ink B cooled down more slowly, which can be related to the fact that it absorbed more energy.

While this temperature is relatively higher than the temperatures reported in other studies, it could be due to the larger diameter of particle size used in this study (100 nm) compared to other studies (20–50 nm) [10, 11]. It has been reported that the melting temperature increases with the increasing diameter of metallic particles, and the melting temperature reaches that of bulk metal if the particle size is larger than 50 nm [12]. Since the required sintering energy is proportional to the melting point of the material, it is possible that the 100 nm copper nanoparticles used in this study requires higher energy to sinter than smaller copper nanoparticles used in other studies.

While the temperature is measured experimentally, the FE model of metallic nanoparticles sintering is developed to verify the temperature at the surface of the sample ink with given experimental conditions. A three-dimensional thermal FE model is developed on ABAQUS Explicit™ using DFLUX subroutine, written in FORTRAN, to calculate the heat flux as a function of time and location within the surface of elements. The surface heat flux distribution is computed based on Gaussian function as follow [13]:

$$Q(x, y) = \frac{3\eta P}{\pi R^2} \text{Exp} \left(-3 \left(\left(\frac{x}{R} \right)^2 + \left(\frac{y}{R} \right)^2 \right) \right), \quad (2)$$

where η is the heat absorption coefficient of the irradiated surface, P is the heat source power, R is the radius of heat source irradiated to the surface of grains and x and y are the distances of a point away from the center of the heat source. Most previous works utilized surface heat flux rather than volumetric heat flux due to the very small layer thickness ($< 100 \mu\text{m}$) of powders [14–17].

In this FE model, it was assumed that the absorption coefficient of copper nanoparticle was constant at

Table 2. Estimated maximum temperature at grain boundary in varying sintering energy based on FE simulations.

IPL Energy (J cm^{-2})	0.86	0.99	1.15	1.29	1.35	1.46
Temperature (K)	461	480	506	526	534	552

63.2% [18], while the energy density was varied from 0.86 to 1.46 J cm^{-2} similar to the experimental conditions. The material properties of copper nanoparticles such as thermal conductivity, specific heat, thermal expansion, Young's modulus, Poisson's ratio, and density were varied as the function of temperature. The known bulk thermal properties ranging from 100 to 830 K were used to develop the FE model [19]. The initial temperature of nanoparticles was considered as room temperature and they were meshed with solid (continuum) elements known as DC3D8 in the ABAQUS element library [20]. It is an 8-node linear brick element with a single degree of freedom (temperature) at each node.

The following assumptions were also applied to the development of the FE model: two nanoparticles of 100 nm diameters were considered with the general contact between them and perfectly constant power supply over the sintering process (i.e. square pulse). The conduction occurred only between the particles, while the heat loss occurred through convection and radiation. There was no atomic bonding or interaction considered in the model. Figure 12 shows the schematic view and the FE model implemented to analyze the thermal distribution during the IPL sintering process. The maximum temperature is achieved at the grain boundary, and the corresponding maximum temperature for the input energy density of 1.46 J cm^{-2} is shown in figure 12(b). Maximum temperature values for additional energy inputs are shown in table 2.

The FE model showed that input power density of 0.86 J cm^{-2} should reach the temperature of 461.5 K,

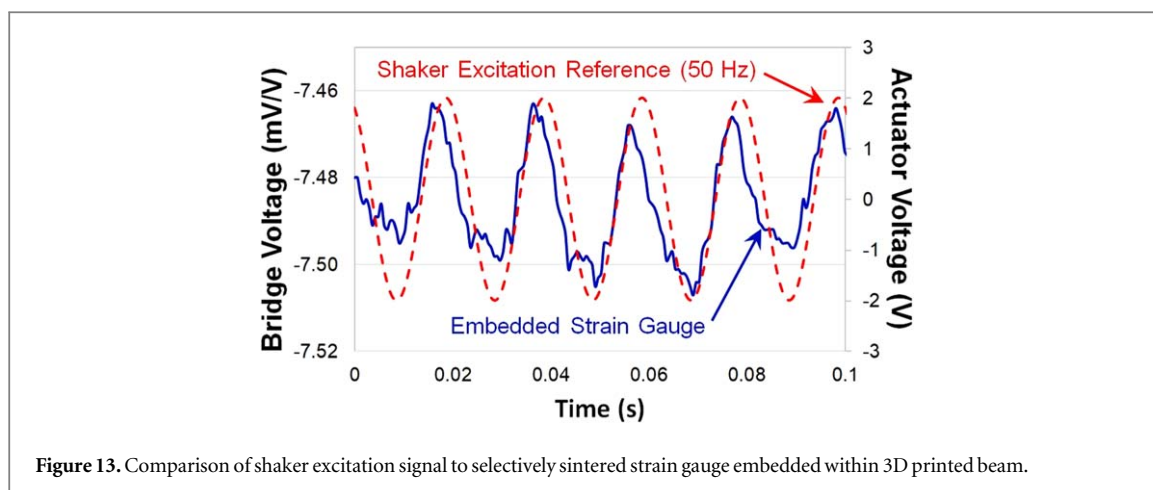


Figure 13. Comparison of shaker excitation signal to selectively sintered strain gauge embedded within 3D printed beam.

strong enough to start the sintering process based on other studies. The experimental results however showed that the sintering of Ink A started at the input power density of 0.99 J cm^{-2} , properly sintering at even higher level of input power density of 1.15 J cm^{-2} based on the thickness of sintered layer. There are many possible reasons for the deviation; there were limitation in the developed model, and there could be the loss of energy due to the reflection of light on reflector panel. The differences in experimental conditions such as the particle diameters and exact composition of ink could have affected the results.

It is also notable that the predicted maximum temperature is localized at the surface, as experimental studies show that the only partial amount of deposited ink was sintered, leaving unsintered area at the bottom of conductive ink film. In conventional heat sintering, there is potential danger of delamination due to the large difference in the coefficient of thermal expansion between the conductive ink (approx. $16 \mu\text{m m}^{-1} \text{ K}^{-1}$) and ABS substrate (approx. $72 \mu\text{m m}^{-1} \text{ K}^{-1}$) even if the temperature was not enough to melt the substrate. In this study, however, the IPL sintering process may not heat the interface to extensively, avoiding the delamination during the sintering process.

3.4. Application as the 3D printed embedded sensor

Embedding conductive ink-based electric circuits and sensors within 3D printed components is the first step toward the full 3D printing of smart electronics and structures. The process also encapsulates the conductive paths and protects them from potential damage and degradation.

This study has shown that the ink B can withstand cyclic bending while its sintering process is safe from thermally damaging the ABS substrate. It is now experimentally verified by printing a strain sensor electric path on the 3D printed half-cantilever, sintered and covered with the other half of the 3D printed cantilever. The cantilever was then excited using a shaker with sinusoidal input signals. The measured strain gauge signal (change in resistance) was plotted and

compared to the shaker excitation signal (see figure 13).

The hybrid copper ink-based strain sensor signal showed a good correlation with the reference when the shaker is excited at 1 and 50 Hz. However, there were noise and discrepancies as some peak values were not shown at 1 Hz. These problems could be accounted for the loss of contact at the sensor-wire joints (i.e. conductive epoxy) and the inconsistent sintering depth.

4. Conclusions

With the advent of 3D printing and printed electronics, the integration of two processes provides synergy for the development of functional devices. In this study, the conductive hybrid copper ink samples were fabricated, then experimentally investigated whether it is applicable for developing a 3D printed embedded sensor. Two types of ink, one with copper nanoparticles coated with a thin silver coating and the other mixed with GnP were compared for its required energy in the IPL sintering process, resulting resistivity, durability in repeated bending as well as the temperature profile over the sintering process. Experimental investigations revealed that the addition of GnP increases the required sintering energy slightly, but the resulting resistivity of the conductive ink was similar at the optimal sintering condition. The cyclic bending tests showed that the conductive ink with GnP had increased durability, which could be explained by the bonding of sintered copper nanoparticles and the GnP shown in SEM images. The *in situ* temperature monitoring of the IPL sintering process and the thermal FE model of IPL sintering process concluded that the maximum temperature of the sample was approximately 550 or 574 K at the top surface. The temperature near the interface with the substrate was not nearly as high, as the observation of the cross-section of sintered samples showed that samples were partially sintered near the top surface. The developed hybrid copper ink was also used to form strain gauges embedded in a 3D printed ABS

cantilever beam. The hybrid copper ink embedded sensor was able to track sinusoidal inputs at 50 Hz.

This study successfully presented a possible application of GnP added hybrid copper conductive ink as an embedded strain sensor, but the investigation was limited to a composition with an arbitrary ratio of materials. In the future, the study will be further expanded to investigate different composition ratios as well as improved sintering process to create a more durable and flexible hybrid copper conductive ink. Also, while the increase in resistance was suppressed in comparison to the hybrid copper conductive ink without GnP, the ink still experienced an increase in resistance over repeated bending cycles. This was possibly due to the formation of inevitable microcracks, with only the difference in severity. Thus, there is a strong motivation for another future study, to develop a self-healing hybrid copper conductive ink, where the broken conductive network could be repaired without the addition of materials.

Acknowledgments

We would like to acknowledge the Natural Sciences and Engineering Research Council (NSERC) of Canada and Alberta Innovates for supporting this research.

ORCID iDs

A Sandwell  <https://orcid.org/0000-0003-3784-324X>

References

- [1] Kamyshny A and Magdassi S 2014 Conductive nanomaterials for printed electronics *Small* **10** 3515–35
- [2] Petherbridge K, Evans P and Harrison D 2004 The origins and evolution of the PCB: a review *Circuit World* **31** 41–5
- [3] Kim H, Dhage S R, Shim D and Hahn H T 2009 Intense pulsed light sintering of copper nanoink for printed electronics *Appl. Phys. A* **97** 791–8
- [4] Yim C, Kockerbeck Z, Jo S B and Park S S 2017 Hybrid copper-silver-graphene nanoplatelet conductive inks on PDMS for oxidation resistance under intensive pulsed light *ACS Appl. Mater. Interfaces* **9** 37160–5
- [5] Etefagh R, Azhir E and Shahmasebi N 2013 Synthesis of CuO nanoparticles and fabrication of nanostructural layer biosensors for detecting *Aspergillus niger* fungi *Sci. Iranica* **20** 1055–8
- [6] Sundar S, Venkatchalam G and Kwon S 2018 Biosynthesis of copper oxide (CuO) nanowires and their use for the electrochemical sensing of dopamine *Nanomaterials* **8** 823
- [7] Yim C, Sandwell A and Park S S 2016 Hybrid copper-silver conductive tracks for enhanced oxidation resistance under flash light sintering *ACS Appl. Mater. Interfaces* **8** 22369–73
- [8] Jyoti K, Baunthiyal M and Singh A 2016 Characterization of silver nanoparticles synthesized using *Urtica dioica* Linn. leaves and their synergistic effects with antibiotics *J. Radiat. Res. Appl. Sci.* **9** 217–27
- [9] Dang T M D, Le T T T, Fribourg-Blanc E and Dang M C 2011 The influence of solvents and surfactants on the preparation of copper nanoparticles by a chemical reduction method *Adv. Nat. Sci.: Nanosci. Nanotechnol.* **2** 025004
- [10] Park S H, Chung W H and Kim H S 2014 Temperature changes of copper nanoparticle ink during flash light sintering *J. Mater. Process. Technol.* **214** 2730–8
- [11] Mittal J and Lin K 2015 Exothermic low temperature sintering of Cu nanoparticles *Mater. Charact.* **109** 19–24
- [12] Yeshchenko O A, Dmitruk I M, Alexeenko A A and Dmytruk A M 2007 Size-dependent melting of spherical copper nanoparticles embedded in a silica matrix *Phys. Rev. B* **75** 085434
- [13] Safari M and Farzin M 2013 Experimental and numerical investigation of laser bending of tailor machined blanks *Opt. Laser Technol.* **48** 513–22
- [14] Roberts I A, Wang C J, Esterlein R, Stanford M and Mynors D J 2009 A three-dimensional finite element analysis of the temperature field during laser melting of metal powders in additive layer manufacturing *Int. J. Mach. Tools Manuf.* **49** 916–23
- [15] Ryu C H, Joo S J and Kim H S 2016 Two-step flash light sintering of copper nanoparticle ink to remove substrate warping *Appl. Surf. Sci.* **384** 182–91
- [16] Patil R B and Yadava V 2007 Finite element analysis of temperature distribution in single metallic powder layer during metal laser sintering *Int. J. Mach. Tools Manuf.* **47** 1069–80
- [17] Fu C H, Sealy M P, Guo Y B and Wei X T 2015 Finite element simulation and experimental validation of pulsed laser cutting of nitinol *J. Manuf. Process.* **19** 81–6
- [18] Kaviany M 2002 *Principles of Heat Transfer* (New York: Wiley)
- [19] Whitaker S 2013 *Fundamental Principles of Heat Transfer* (Amsterdam: Elsevier)
- [20] Chen X, Duan X, Jiang G and 2019 Numerical investigation of transient temperature field on the selective laser melting process with Al6063 *IOP Conference Series: Materials Science and Engineering* **667** 1–6